Polyamide 6 Nanocomposites Incorporating Cellulose Nanocrystals Prepared by *In Situ* Ring-Opening Polymerization: Viscoelasticity, Creep Behavior, and Melt Rheological Properties

Shahab Kashani Rahimi, Joshua U. Otaigbe
School of Polymers and High Performance Materials, the University of Southern Mississippi, Hattiesburg, Mississippi

The creep behavior and solid and melt linear viscoelasticity of novel polyamide 6 (PA6) nanocomposites reinforced with cellulose nanocrystals (CNCs) prepared via *in situ* anionic ring-opening polymerization (ROP) were investigated to accelerate research efforts to develop new polymeric materials with improved properties for lightweight, load-bearing applications. The obtained results showed that incorporation of relatively small amounts of $\leq$ 2wt% CNCs into the PA6 thermoplastic matrix gave nanocomposite samples with significantly enhanced creep and viscoelastic materials functions of the PA6 as indicated by lower creep strain, lower creep compliance, improved elastic recovery after removal of load, and reduced Arrhenius activation energies for time-dependent viscoplastic flow. The obtained results were analyzed and interpreted by theoretical equations for predicting the viscoelasticity and creep behavior of polymeric systems. The melt rheological properties showed enhanced melt strength and elasticity. The formation of a percolated network structure of CNC was revealed by morphological observations that were consistent with the dynamic structure break-up and reformation rheological experiments. The stiffness, rigidity of the CNCs along with their special ROP-facilitated intrinsic strong chemical interactions with the PA6 matrix is believed to be responsible for the observed superior creep and viscoelastic materials functions even with very little CNC concentration. POLYM. ENG. SCI., 56:1045–1060, 2016. © 2016 Society of Plastics Engineers

INTRODUCTION

Polymer nanocomposites are an important class of polymer based materials that have found numerous applications in science, engineering and advanced technologies due to their unique properties that are attainable through the combination of specific characteristics of the polymer matrix and the relatively small concentration of nano-filler reinforcements. In this context, engineering thermoplastics like polyamide 6 are currently of academic and industrial research interest due to their superior mechanical properties, wear and chemical resistance, and good thermal stability [1, 2]. However, in a similar way to other thermoplastic polymers, they undergo viscoelastic deformation and creep under load when used in load bearing applications.

Recently, addition of various kinds of nanoparticles into polymer matrices has been shown to effectively improve the creep resistance of the polymer matrix to an extent that depends on the type, shape and concentration of the nanoparticles. For example, Yang and co-workers [3] reported that low content (i.e., 1 wt%) of spherical (TiO_2) and platelet-like (organoclay) particles in polyamide 6,6 improved the creep resistance of the polymer matrix even at elevated temperatures and different stress levels.

A number of research studies that aim to improve the physical properties of polyamide 6 (PA6) matrix through the addition of various nanoparticles such as silica [4], organoclays [5], graphene [6] and carbon nanotubes [7] have been reported. For example, nanoclay has been found to improve the viscoelastic and rheological properties of PA6 matrix [8], where it was found that addition of a small volume fraction of clay to PA6 reduced the creep strain of both water saturated and dry PA6 samples through molecular level viscous slippage inhibition effect.

More recently, there has been a great interest in both the scientific and industrial communities in application of natural fibers from renewable agricultural resources as the reinforcing additive in polymer composites. This interest is primarily due to the low cost and abundance of plant-based cellulose fiber resources, low density of the final composite part, low wear of processing equipment, and biodegradability [9, 10]. Therefore, this cost effectiveness, lightweight, renewability and environmental sustainability compared to traditional glass or carbon fiber composites have made these natural fibers very attractive for polymer composite applications. Gong et al. [11] developed composites of polyvinyl acetate reinforced with cellulose nanofibers. Their results showed that the final creep deformation of the matrix can be reduced by using $1-10\%$ of CNFs. They also showed that the activation energy of the molecular motion through analysis of α-transition tan δ peak measured at different frequencies could be increased by increasing the CNF content. Spoljaric et al. [12] used microcrystalline cellulose (MCC) as reinforcing filler in polypropylene matrix. They found that MCC can effectively reduce the creep strain of polypropylene at various loading levels as well as increase the storage modulus and glass transition temperature. The MCC was also found to increase the elastic recovery of strain in recovery process and

Correspondence to: J.U. Otaigbe; e-mail: Joshua.otaigbe@usm.edu
Contract grant sponsor: U.S. National Science Foundation Division of Civil, Mechanical and Manufacturing Innovation; contract grant number: CMMI-1161292; contract grant sponsor: Office of International and Integrative Activities; contract grant number: IIA-1346898.
Part of this work was orally presented at the SPE-ANTEC Dubai 2016 in partnership with GPCA Plasticon in United Arab Emirates; the 250th ACS national meeting and exposition (2015) in Boston, USA; and the SPE-ANTEC 2015 in Orlando, USA.
DOI 10.1002/pen.24335
Published online in Wiley Online Library (wileyonlinelibrary.com).

reduce the permanent deformation which is an important factor in dimensional stability of polymer materials when the load is removed. Their results showed that upon application of a reactive interfacial modifier, the reinforcing effect can be significantly improved.

Cellulose nanocrystals (CNCs) have gained particular interest among bio-derived nano-fillers due to their exceptional mechanical properties having a longitudinal modulus in the range of 100–150 GPa with an average value of 130 GPa that is almost equivalent to that of aramid fibers [13, 14]. CNCs have been used as an effective reinforcing agent in a number of polymer systems including polyurethanes [15], poly lactic acid (PLA) [16], epoxy thermosets [17], and polyvinyl acetate adhesives [18]. In a study on shape memory polyurethane reinforced with CNCs [19], a significant enhancement in creep resistance was observed by a reduction of around 40% of the total creep strain with only 1% of CNC in the composite. Iyer et al. [20] developed low-density polyethylene (LDPE)/CNC composites using solid state pulverization technique. The excellent dispersion of CNCs in this hydrophobic LDPE matrix obtained by this mixing strategy resulted in effective property enhancement of mechanical properties and creep resistance.

Despite this reported successes in the application potential of cellulosic fibers as reinforcement for polymers, their use in engineering thermoplastic composites have remained a challenge due to the high melting point (and thus processing temperature) of these thermoplastics such as polyamide 6 ($T_m \sim 220$°C) which overlaps with the thermal degradation temperature of CNCs [21]. Consequently, most nanocomposites containing these nanocrystals have been made by either using hydrophobic polymers with low melting points, or by solvent casting techniques with less than optimal impact [22, 23]. Recently, in a series of studies, Kiziltas et al. [24, 25] reported a melt processing strategy that has been used to blend microcrystalline cellulose with polyamide 6 matrix in a Barbender® mixer. The rheological characterization of the composite showed an increase in melt elasticity and viscosity at high MCC content; and the crystallization studies showed some molecular motion inhibition in crystal formation in presence of MCC particles. Carolina-Correra et al. [26] used a combination of solvent casting and melt processing method to fabricate nano-cellulose reinforced PA6 composites and their obtained results showed promising reinforcing capability even at very low CNC content of 1 wt%. This observed reinforcement efficiency is primarily due to the good dispersion of CNC particle and good protection of CNCs by the cast nylon chains in the melt processing step against thermal degradation.

In addition to the melt processing techniques already described, anionic ring-opening polymerization (ROP) of ε-caprolactam has been used in resin infusion type processes [27] to fabricate PA6 based macro- and nano-composite. In a series of relatively recent studies by Rijswijk et al. [28–31] on glass fiber-reinforced PA6 composites and other studies by other researchers on clay [32], zinc [33], and carbon nanotube [35] reinforced PA6 composite, the authors showed that by using the ROP reaction, an effective dispersion of particles (or excellent fiber wet out in the case of macro-fibers [27]) could be achieved by the selection of optimized ROP and processing conditions. An example of the efficiency of this ROP technique was reported by Tung et al. [35] where rheological experiments were used to compare clay-reinforced polyamide 6 nanocomposites prepared by both melt blending and *in situ* ROP technique. Their results indicated that ROP facilitated the fabrication of composites with improved properties due to better dispersion of clay.

The work described in this article is part of a long-range research effort to develop novel composite materials based on polyamide 6 matrix reinforced by cellulosic fibers using the ROP technique because the relatively low polymerization temperature (~150°C) minimizes the thermal degradation of the cellulosic fibers that is observed in conventional polymer processing methods like extrusion and injection molding as already described. In addition, the low viscosity of the starting reactive monomeric system allows for better dispersion of nanoparticles. The aim of this article is to report on the preparation, viscoelastic, and creep behavior of PA6/CNC nanocomposite prepared by *in situ* ROP reaction using optimal prescribed conditions with improved results. The obtained results are analyzed and interpreted within the context of a number of extant theoretical equations that pervade the literature for predicting the viscoelasticity and creep behavior of polymeric systems. It is hoped that the interesting results of this study will provide a basis for further exploitation and better understanding of the facile strategy of developing new engineered thermoplastic nanocomposites reinforced with cellulosic fibers with improved properties for a number of load-bearing applications with enhanced benefits.

In addition to their superior mechanical properties like high stiffness and high surface area available for interaction with matrix, CNC particles have a low density compared to conventional reinforcements such as silicates, glass fiber and carbon fiber. Therefore, the PA6/CNC nanocomposite material of this study is lighter and has superior performance properties for targeted metal replacement component spare parts in vehicular applications where light weighting while meeting CO_2 reduction standards is crucially important.

EXPERIMENTAL

Materials and Preparation of Nanocomposites

The caprolactam monomer used was an AP-Nylon® caprolactam grade (purchased from Brueggemann Chemical, Pennsylvannia) with low moisture content (<100 ppm) suitable for anionic ring-opening polymerization. The phenyl isocyanate and sodium hydride used were purchased from Aldrich and used as-received. Bleached kraft pulp paper (from southern yellow pine) with 99–100 wt% cellulose (lignin-free pulp) was obtained from Weyerhaeuser and used as the starting material for the preparation of cellulose nanocrystals (CNCs).

In this study, cellulose nanocrystals were prepared by sulfuric acid hydrolysis of bleached cellulose paper (kraft pulp) following the method reported by Capadona et al. [36] with some modifications. The paper was cut into small pieces and blended at high speed with de-ionized water (20 g/L) to achieve a lumpy cellulose pulp followed by placement in a glass reactor in an ice bath. Acid sulfuric (98%) was slowly added to the cold suspension to reach a concentration of 35 v/v% of acid in total suspension. The mixture was then heated to 50°C and stirred for 3.5 h. The obtained suspension was subsequently quenched with 10-fold excess of deionized (DI) water and filtered over fine gritted

 DOI 10.1002/pen

glass filter and washed slowly with DI water until the running water showed pH $\sim$ 6. The resulting mixture was decanted to remove the unhydrolyzed fibers and then centrifuged (5 cycles) at 3000 rpm for 10 minutes to concentrate the CNCs. The nanocrystals were recovered by freeze-drying of the suspension and were neutralized with 2 nM NaOH solution to convert the surface sulfonic acid groups to sodium salt (indicated by pH neutrality of the CNC dispersions). The obtained neutralized CNCs were dried overnight in a vacuum oven at 100°C prior to preparation of the nanocomposite samples.

Nanocomposites were prepared by *in situ* ring-opening polymerization of caprolactam monomer in the presence of CNCs. For this purpose, the CNCs were dispersed in the monomer at 0.6, 1, and 2 wt% CNC concentrations by high-speed agitation (700 rpm) for 30 minutes and sonicated for 25 min at 85 − 95°C. The ROP activator was synthesized separately by reaction of the phenyl isocyanate with caprolactam under inert atmosphere for 1 h at 95°C. The ROP initiators were prepared by addition of sodium hydride to monomer under nitrogen atmosphere. The initiator and activator (1.5 mol% and 1.2 mol%, respectively) were then added to the CNC-containing monomer dispersion and the mixture was allowed to polymerize at 150°C for 30 min in a disk shaped mold under vacuum. The conversion of the monomer into polymer was determined by extracting the unreacted monomer in a Soxhlet apparatus using boiling water as the extracting liquid for 9 h. The nomenclature used here for the test nanocomposite samples is *x*% CNC where "*x*" denotes the CNC content in weight percentage in the composite sample. The prepared composite plates were cut and granulated into small pieces that were used to prepare standard test samples for the various measurements as described in the following sections. Thermal analysis via thermogravimetric analysis (TA Instruments Q500 TGA) were performed to analyze the thermal stability of the cellulose nanocrystals at polymerization temperature of 150°C and no thermal degradation of CNCs were detected.

Test Sample Preparation

Samples for dynamic mechanical analysis (DMA) tests were prepared from the granulated composite samples obtained from the polymerization mold by compression molding. Rectangular bars with dimensions of 3.2 × 12.6 × 20 mm^3 were compression molded in MTP-24 Tetrahedron® laminating press at 235°C under 5 tons (or 49 kN) of force. The composite granules were dried overnight in a vacuum oven at 80°C after monomer extraction prior to compression molding. The obtained rectangular bars were dried overnight at 80°C prior to DMA tests that were performed under constant flow of dry nitrogen in order to prevent the interference of moisture absorption of samples in the test data acquisition and analysis. For creep tests, rectangular bars with 1.08 × 14.90 × 20 mm^3 dimensions were injection molded using a Daca® micro-injector bench-top injection molding machine using a barrel temperature of 235°C and a mold temperature of 120°C followed by ambient cooling of the mold after the injection molding. The injection molded bars were dried overnight in a vacuum oven at 80°C and stored in the desiccator until required for testing.

Atomic Force and Scanning Electron Microscopy. Atomic force microscopy (AFM) Images of the cellulose nanocrystals (CNCs) were captured using a Multimode scanning probe microscope (Veeco® instruments). A silicon probe with 125 μm silicon cantilever with a nominal force constant of 40 N/m was used in tapping mode surface topography in this study. The AFM test specimens were prepared by drop-casting of CNC dispersion from ethanol on Mica surface by spin-coating (3000 rpm) followed by nitrogen blow-drying. The microstructure of the nanocomposite samples was studied by a Sigma field-emission scanning electron microscope (ZEISS®, USA) using a 5 kV accelerating voltage. The imaging was performed on cryo-fractured surfaces of the nanocomposite samples sputter-coated with silver for enhanced conductivity.

Dynamic Mechanical and Creep Testing

Dynamic mechanical tests were performed using a Perkin Elmer Diamond® DMA using a dual cantilever mode to study the bulk viscoelastic properties of the samples as functions of temperature and frequency. Dynamic viscoelastic properties were measured in the range of −20 to 200°C at a constant frequency of 1 Hz; and the frequency sweep tests were performed at 30°C in the frequency range of 0.05 − 100 Hz following standard methods.

A Q800 TA® Instruments DMA was used in three point-bend geometry for the creep tests and analysis. The creep tests were performed at 25, 50, 75, 90, and 105°C under a constant stress of 4 MPa that was previously determined to be in the linear viscoelastic region. For each test, a new sample was used and the strain was measured as a function of time. The samples were pre-equilibrated at the desired temperature for 5 min prior to the application of the stress for 60 min followed by 60 min of recovery after removal of the applied stress.

Melt Rheological Characterization

Melt rheological measurements were performed both in the strain-controlled and stress-controlled modes. Dynamic frequency sweep experiments were carried out on an ARES® rheometer using 25 mm parallel plate geometry, a gap of 1mm and a linear strain of 1.25% that was predetermined from a strain sweep test. For the time sweep test, a frequency of 5 rad/s was used. Stress-controlled experiments were done using a DHR2® TA-instruments rheometer and 25 mm diameter parallel plate geometry with a gap of 0.8 mm while for the steady shear flow curve experiments, a cone-and-plate geometry was used in order to maintain a constant shear rate throughout the sample. All the tests were performed under nitrogen atmosphere and the temperature was kept constant at 226°C to ensure a fully molten system and negligible degradation of the samples that was monitored as a less than 6% reduction in G' under the test conditions used. A thermal soak time of 40 s was found to be sufficient to eliminate the residual stress in the samples from the polymerization process, yielding reproducible results that typically replicated to within about 10% from sample to sample. In order to study the structure break-up and recovery in the samples, the samples were pre-sheared at desired shear rates (i.e., 0.1, 1, and 10 s^{-1}) and subsequently subjected to a dynamic time sweep test with a frequency of 5 rad/s and a linear strain of 1.25% and the evolution of viscoelastic properties (G' and G'') over time were obtained.

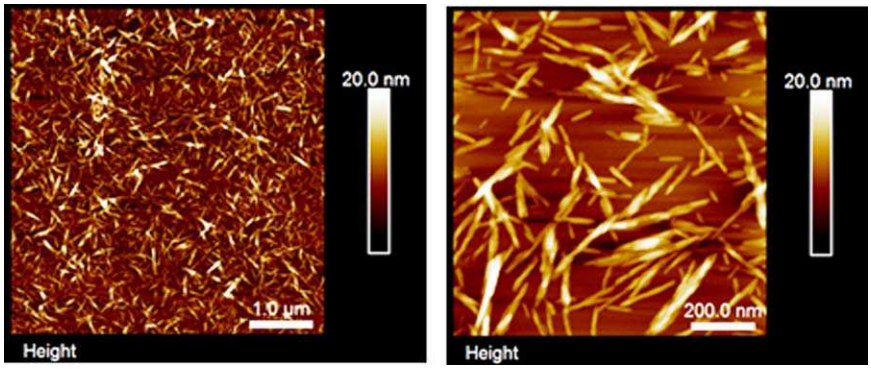

FIG. 1. AFM images of CNCs prepared by acid hydrolysis. [Color figure can be viewed in the online issue, which is available at wileyonlinelibrary.com.]

RESULTS AND DISCUSSION

Cellulose Nanocrystal Preparation and In Situ *Polymerization*

An AFM image of the prepared cellulose nanocrystals (CNCs) is shown in Fig. 1. Typically in the acid hydrolysis process, the noncrystalline regions (mostly amorphous) of the lignocellulosic fiber are removed by dissolution in the acid medium. This amorphous region is mainly composed of the paracrystalline regions of hemicellulose and the lignin-based portion of the cellulosic fiber. The cellulose starting material, concentration of sulfuric acid, and temperature of hydrolysis determines the final aspect ratio of the CNCs. As evident in Fig. 1, the obtained CNCs had an aspect ratio of 14–20.

The conversion of the ε-caprolactam monomer in the different composite samples is shown in Fig. 2a. As can be seen in this figure, the monomer conversion ranged from 98.5% (PA6) to 95.8% (nanocomposite with 2% CNC). Increasing the CNC content is seen in Fig. 2b to be associated with the evolution of brown color in the composite samples most likely due to the polymerization reaction inhibition effect of CNC particles. It has already been shown that preparation of PA6 based composites by *in situ* ring-opening polymerization in presence of different types of reinforcing fillers such as organoclay [32], TiO_2 [37], metal nanoparticles [38], and glass fibers [28] results in lower conversions of monomer due to the deactivation of growing anionic chain by proton donating species. In the case of cellulose nanocrystals, the deactivation of growing anions is ascribed to bound water molecules on the hydroxyl rich surface of cellulose which can act as an effective proton donating species during the anionic polymerization reaction. Although the CNCs were thoroughly dried overnight in a vacuum oven and immediately kept under dry nitrogen atmosphere until required for use, the remaining bound-water on the surface may be difficult to completely remove and may therefore lower the polymerization yield. In addition, the surface hydroxyl groups of the CNC may act as proton donating species and consequently deactivate the anionic centers on the growing polymer chains thereby lowering the final conversion. It is worthy to note that upon sulfuric acid hydrolysis and neutralization process, the most active hydrogen donating species (i.e., the methylol groups on the CNC surface) are converted to sodium sulfonate groups which in turn eliminates the proton donating ability of the methylol groups. Therefore, the proton donation from these methylol groups is less likely to be the primary reason for lower conversion of the polymerization reaction. It should also be noted that the other hydroxyl groups on the cellulose surface are less accessible to the growing PA6 chain anion due to the significant steric hindrance imposed by cellulose backbone structure. These potential inhibition mechanisms are depicted in reaction schemes of Fig. 2c.

Morphological and Dynamic Mechanical Analysis. The microstructures of the samples were studied by SEM imaging of the cryo-fractured surfaces. As shown in Fig. 3, it is clearly evident that a good dispersion of the CNC in PA6 matrix was obtained using the *in situ* ROP technique. In fact, a dual structural feature of the CNC particles in the matrix can be seen where the dispersed individual whiskers tend to form a more clustered network-like structure with increasing CNC content. Clearly, the cellulose nanocrystals show a strong tendency to interact with each other and form larger "bundles" and fibrillar structures (see Fig. 3). As the content of CNC is increased from 0.6 to 2 wt%, initially, the whiskers (i.e., single rod-like crystals in the form of filaments with no dislocations) of CNCs tend to form small clusters promoted by the edge-edge effect rather than side-ways aggregation. This is primarily due to the less number of negatively charged sulfonate groups on the CNC surface at the edges that promotes this type of flocculation. In the sample with 2% of CNC, it is clearly seen that the whiskers are in fact, forming a 3D structure by interconnected bundles. These bundles are larger than the length scale of individual whiskers and are clearly formed by clustering of individual whiskers. The effect of this interconnected network of fibrillar structures will be described later in the sections on structural and melt rheological properties of the nanocomposites.

The dynamic mechanical characterization was performed on the neat PA6 and nanocomposite samples to evaluate the effect of addition of CNCs on the thermomechanical properties of the PA6 matrix. The temperature dependency of storage modulus of the PA6 matrix upon addition of the cellulose nanocrystals is shown in Fig. 4a. The storage moduli of the samples at representative temperatures of 30°C and 80°C that are respectively below and above the glass transition temperature of the neat PA6 are shown in Table 1 (values are averages of 3 replicates). Clearly, addition of very little amount of cellulose nanocrystals increased the storage modulus of the neat PA6 matrix. For

 DOI 10.1002/pen

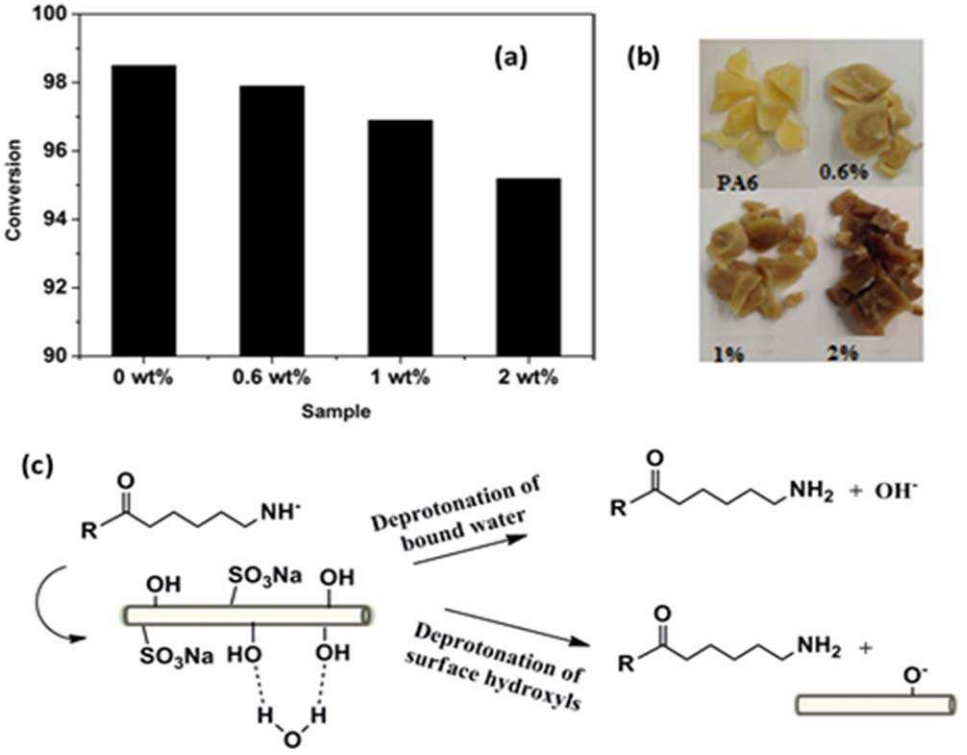

FIG. 2. (a) Monomer conversion in the composite samples and (b) change in color of the composites with addition of varying CNC contents. (c) Proposed mechanism of termination of propagating anionic centers by proton abstraction. [Color figure can be viewed in the online issue, which is available at wileyonlinelibrary.com.]

example, with the addition of 2 wt% of the CNCs, the modulus increased from 1.95 to 2.6 and from 0.52 to 0.74 GPa at 30° and 80°C, respectively (see Table 1). Cellulose nanocrystals are known to be highly stiff particles with a longitudinal modulus of up to 150 GPa and shear modulus of 5 GPa [39, 40]. Therefore, the obtained increase in modulus is ascribed to the

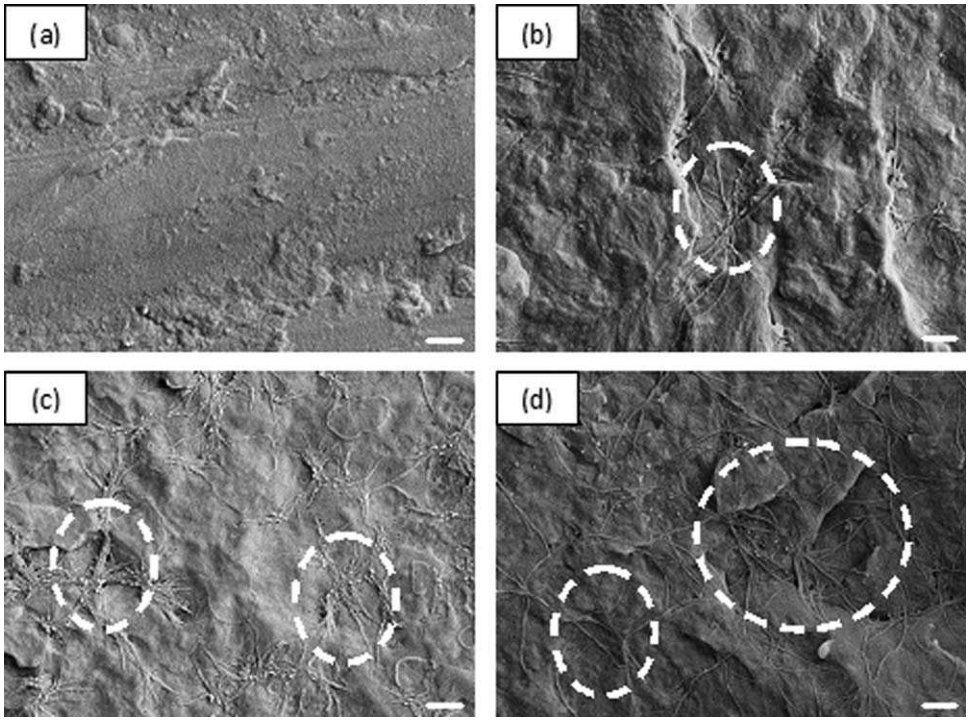

FIG. 3. Scanning Electron Micrographs of cry-fractured surfaces of (a) PA6, (b) 0.6%CNC, (c) 1%CNC and (d) 2%CNC nanocomposites. (The scale bar shown is 1 μm).

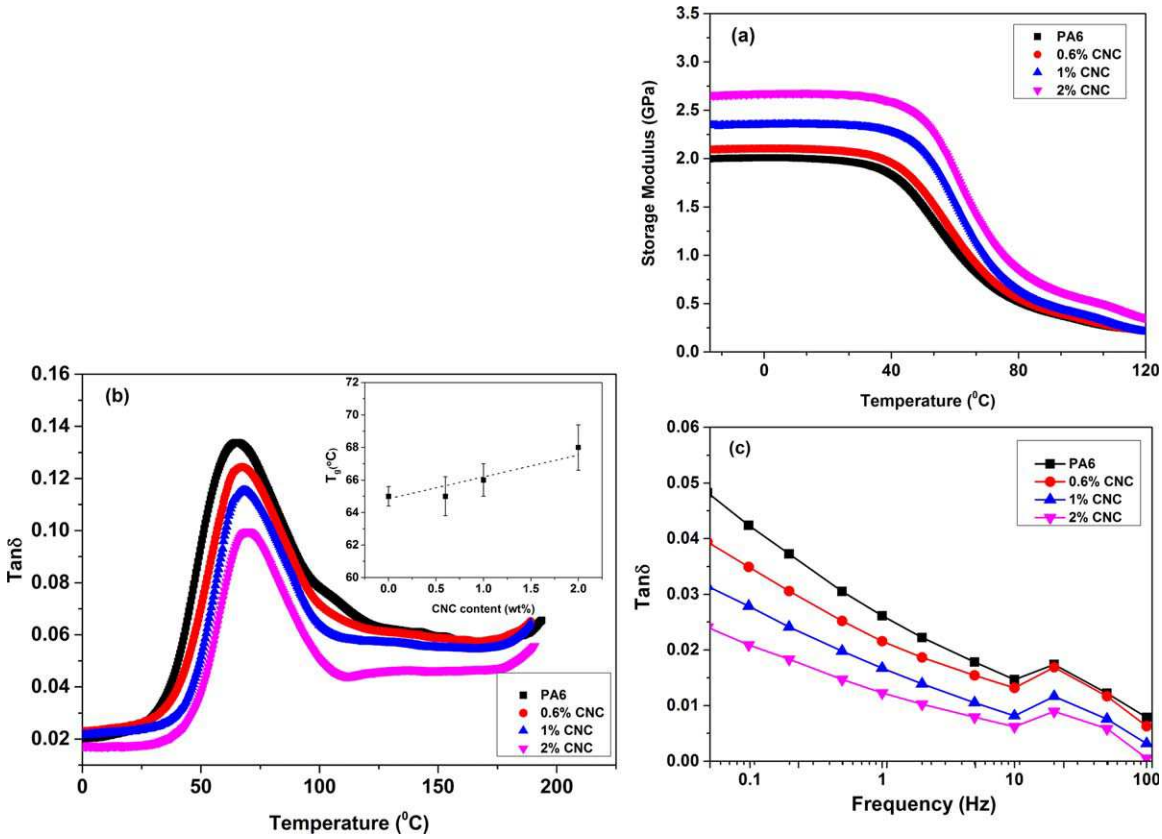

FIG. 4. Variation of (a) storage modulus with temperature, (b) tan δ with temperature and (c) tan δ with frequency. Change in glass transition temperature with CNC content (dotted lines) is shown in Figure 4c inserted figure. [Color figure can be viewed in the online issue, which is available at wileyonlinelibrary.com.]

presence of the rigid elastic CNCs even at low concentrations ($\leq$2 wt% CNC) that enhanced the rigidity of the matrix by making the molecular motion of polymer chains more difficult. It should be mentioned here that our DSC data (not shown) indicate that upon incorporation of CNCs into PA6 matrix, the overall crystallinity of the system reduces from around 45.9% in pure PA6 to 38%, 37% and 30.9% in nanocomposites with 0.6,1 and 2 wt% of CNC, respectively. It is worthy to note that the melting peak of the α-type crystals (occurring at around 220.5 $\pm$ 0.5°C) of the PA6 does not seem to be significantly affected by the presence of the CNCs. However, a clear evolution of the melting peak corresponding to γ-type crystals at 216 $\pm$ 1°C is evident as the CNC content is increased, implying a development of the less ordered crystal structure of polyamide chains on the CNC surface. A more detailed thermal analysis and crystallization kinetics of PA6/CNC nanocomposites is the subject of a future publication that will be published elsewhere. However, it should be noted that based on the thermal analysis study just mentioned, the observed reduction in overall crystallinity is not consistent with the stiffening of the PA6 as seen in DMA results, suggesting that the CNC particles and their reinforcing effect is responsible for the observed enhancement of properties.

The variation of the loss tangent (tan δ) with respect to temperature is shown in Fig. 4b. The glass transition temperature can be determined from the temperature corresponding to the maximum peak of tan δ because it is the temperature at which the molecular motion of the polymer main chain segments is maximized. Note that polyamide 6 has three well-known α-, β-, and γ-relaxation processes. However, in this study, the $\beta-$ and γ-relaxations are out of the temperature range studied. Typically, the α-relaxation peak temperature is associated with the glass transition temperature [41]. Therefore, it is evident from Fig. 4b that addition of the cellulose nanocrystals to PA6 only slightly increased the glass transition temperature. It is worthy to note that addition of various nano-fillers such as organoclay aluminosilicates [9, 42, 43], carbon nanotubes [44] and silica nanoparticles [45] to PA6 has been reported in the literature to either increase or decrease the glass transition temperature of PA6 to an extent that depends on the interfacial interaction and compatibility between the nano-filler and the PA6 matrix.

There are a number of distinctive features in the temperature dependency of tan δ in Fig. 4b. The slight increase in the α-peak temperature for the highest CNC content composite shows that addition of a small fraction of CNCs imposes restriction on chain mobility and therefore results in the slight increase in the T_g. Considering the fact that PA6 is a semi-crystalline polymer; this chain movement restriction originates mainly in the amorphous regions of the polymer structure. CNCs possess hydroxyl group-rich surfaces that are available to form strong hydrogen bonds with the PA6 matrix. This suggests that during the course of polymerization, the simultaneous crystallization of polymer chains in the solid state may disrupt the crystalline structure of the polymer in the areas where the particles are located in the composite. This point is consistent with the reported observation

 DOI 10.1002/pen

TABLE 1. Average values of storage modulus at two different temperatures as well as tan δ peak characteristics.

Sample/property	G' at 30°C (GPa)	G' at 80°C (GPa)	tan δ peak temp (°C)	tan δ maximum height
PA6	1.95	0.52	65	0.134
0.6%CNC	1.98	0.45	65	0.124
1%CNC	2.3	0.54	66	0.115
2%CNC	2.6	0.74	68	0.099

by Kiziltas et al. [25] that addition of cellulose reduces the overall crystallinity of PA6-based composite materials. As a consequence, the amorphous regions in the polymer structure can interact tightly with CNC surface through H-bonding to form a rigid fraction in the vicinity of the particles. This "stiffening" of polymer chains results in the hindered molecular relaxation and motion resulting in the observed slight increase in the T_g already mentioned. It can also be seen in Fig. 4b that as the concentration of cellulose nanocrystals increases in the matrix, the height of the tan δ peak is reduced. This observed decrease in the height of the tan δ peak is attributed to the reduction in damping characteristic of the polymer chains which is typically caused by incorporation of highly stiff and elastic particles that resist the dissipation of energy under load and improve the elastic nature of the composite.

The frequency dependency of tan δ at 30°C is shown in Fig. 4c showing that the obtained tan δ values decreased as the CNC content was increased throughout the whole frequency range studied. As can be seen in this figure, the reduction in tan δ is more pronounced in the low frequency domain, and as the CNC content is increased, the nanocomposites showed relatively lower dependency on the frequency. We propose a number of possible reasons for this observation. The loss tangent of the nanocomposite which is a measure of the viscoelastic energy damping characteristics of the constituents is expected to be reduced by the presence of the rigid CNC whiskers dispersed in the matrix. In addition, the strong interaction between the polyamide 6 and CNC surface will significantly reduce the chain mobility at the interface and reduce the conversion of mechanical energy to heat at polymer-particle interface as the polymer and particle slide past one another resulting in dissipation of energy. This last point is consistent with the relative increase in T_g of the nanocomposites with increasing CNC content. Further, the morphological observations showed the development of a more homogenous network of interconnected CNC whiskers that is capable of reducing the heat dissipation by stress variation due to non-homogeneity of viscoelastic constituents (i.e., the matrix and CNC with different elasticities).

Creep and Recovery Behavior

Figure 5 shows the creep deformation and recovery process of neat PA6 together with the nanocomposite samples containing 0.6, 1, and 2 wt% of cellulose nanocrystals at three different temperatures. An applied stress of 4 MPa was chosen for the creep measurements to ensure the linear viscoelastic deformation region. The overall creep process is made up of the instantaneous deformation (known as the initial creep), the primary creep, and the secondary rupture creep. The experimental conditions were set so that the "rupture" did not take place for the purpose of theoretical modelling of the data.

Expectedly, as Fig. 5 illustrates, for all the neat matrix and nanocomposite samples, the creep strain increases with increasing temperature. For example, in the case of the neat PA6 matrix, the final deformation after 1 h of creep increased by 467% when the temperature was increased from 25 to 105°C. It also clearly evident in Fig. 4 that throughout the temperature range studied, the total creep strain is much lower for the nanocomposite samples compared to that of the matrix. By increasing the CNC content in the composite, the creep resistance improved and the final creep strain decreased. It is worthy to note that the temperature is comparatively less effective on the nanocomposite samples in terms of the effect on the creep strain compared to that of the neat matrix. In other words, the nanocomposite samples (especially the 2 wt% CNC sample) showed less dependence of creep strain on the temperature. The fact that the creep resistance of the samples was improved by addition of CNCs is due to the elasticity and rigidity of the nanocomposite samples. Note that in the presence of stiff cellulose nanocrystals, the polymer molecules show less tendency toward the deformation and chain slippage and can resist the applied load more effectively. From the evolution of the creep curves depicted in Fig. 4 it can be seen that in the second stage of creep which corresponds to the viscoelastic motion of the material, the sample deformation is significantly reduced with increasing CNC content. For example, by addition of 2 wt% of CNC, the creep strain of the PA6 matrix shows a reduction of 48% at 25°C while at the 105°C, this reduction in creep strain is more than 61%. This finding points to the fact that at higher temperatures where molecular motion is facilitated by thermal energy of polymer chains, the presence of rigid stiff CNCs significantly improves the creep resistance of the PA6 thermoplastic matrix. Similar effects were observed in the work of Gong et al. [11] and Spoljaric et al. [12] where the incorporation of cellulosic nanofiber in poly (vinyl acetate) and micro-crystalline cellulose in polypropylene matrix resulted in significant improvements in the creep resistance of the polymer matrix.

For the creep recovery process in Fig. 5, the following three distinctive features are clearly evident in the recovery strain. A fast step-wise recovery which corresponds to the elastic recovery of the polymer chains when the load is removed from the sample. This is then followed by a viscoelastic recovery over time which then ends with a certain irrecoverable strain at the end of the experiment. This last stage is related to the pure viscous movement of the polymer chains which is not recoverable after removal of the load and often referred to as the permanent deformation. As expected, in the permanent deformation stage, increasing the temperature for all the samples increased the permanent deformation and reduced the ability of the material to recover the deformation elastically. This observation is due to relatively easier viscous flow and plastic deformation that is

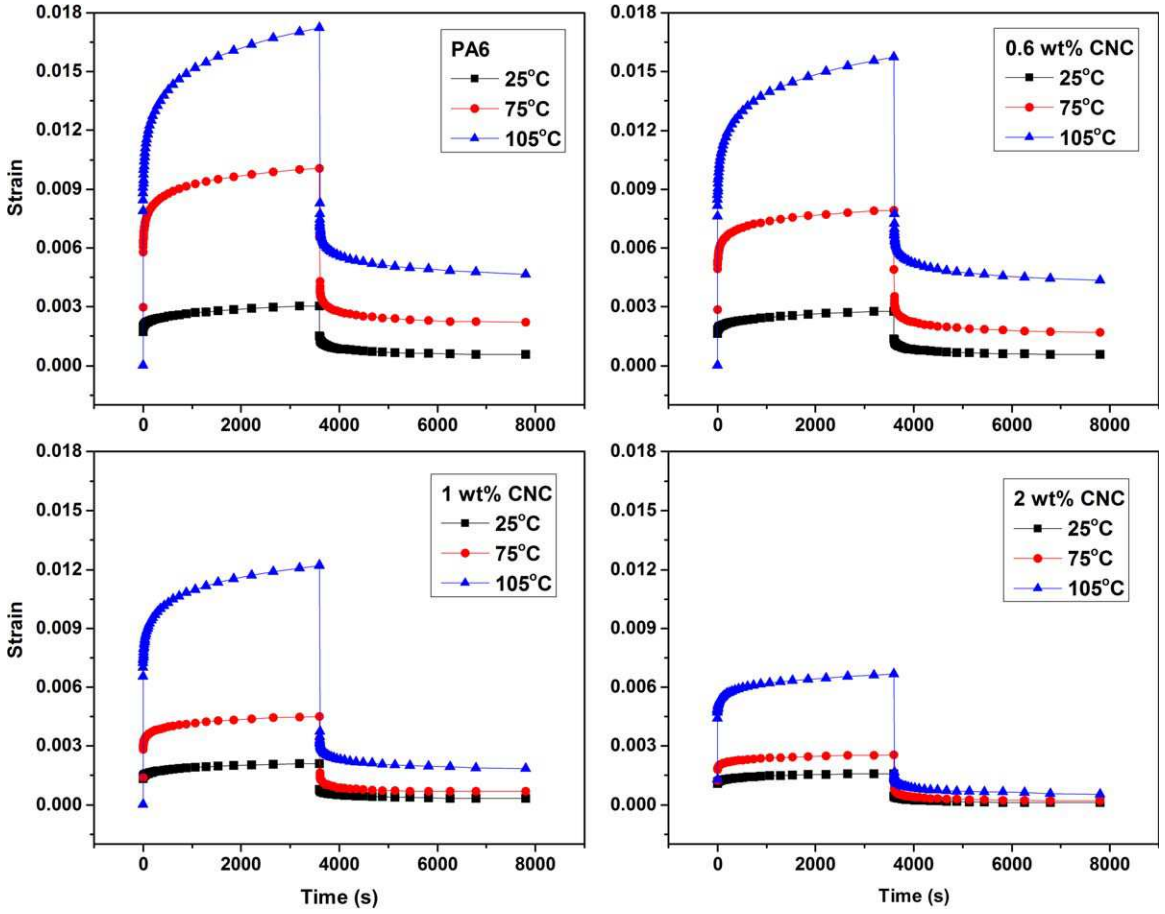

FIG. 5. Variation of creep strain versus temperature for: (a) neat PA6, (b) 0.6%CNC composite, (c) 1%CNC composite and (d) 2%CNC composite. [Color figure can be viewed in the online issue, which is available at wileyonlinelibrary.com.]

exacerbated at higher temperatures. The addition of the CNC particles to the matrix enhanced the nanocomposite's capability to recover the strain and reduced the permanent deformation, clearly showing the elasticity contribution of the cellulose nanocrystals to the physical structure of the composite.

It is instructive to distinguish the instantaneous creep deformation upon application of the stress from the creep deformation that takes place over time. In this context, the time-dependent creep compliance (which excludes the instantaneous elastic deformation in the beginning of creep process) is an important variable through which the information about the effect of particles on viscous behavior and chain slippage of the samples can be directly gleaned. Here, the obtained creep compliance values were reduced by the initial compliance, J_o (which is due to the instantaneous elastic deformation) at each specific time and then normalized by the initial compliance value. The obtained results are presented in Fig. 6. This figure shows that the overall time-dependent creep compliance of the samples is reduced as the CNC content within the nanocomposite is increased.

The variation of strain rate with time is shown in Fig. 6. By comparing the strain rates of the samples, it can be clearly seen that addition of CNC into PA6 matrix reduced the strain rate during the creep period studied. In other words, for the sample with higher CNC content, the rate of deformation at an identical time interval is lower compared to that of the matrix. This observed result is closely associated with less dependence of the viscoelastic creep behavior with addition of the cellulose crystals which is ascribed to the result of enhanced stiffness and elasticity caused by incorporation of the rigid CNCs. The

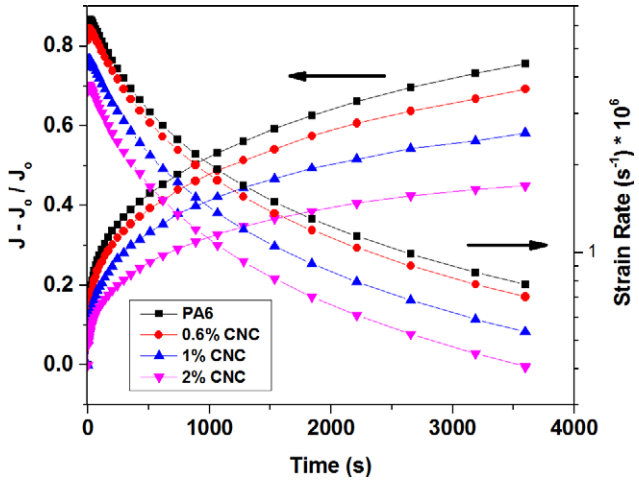

FIG. 6. Normalized time-dependent creep compliance and Strain rate as a function of time for neat PA6 and nanocomposites. [Color figure can be viewed in the online issue, which is available at wileyonlinelibrary.com.]

DOI 10.1002/pen

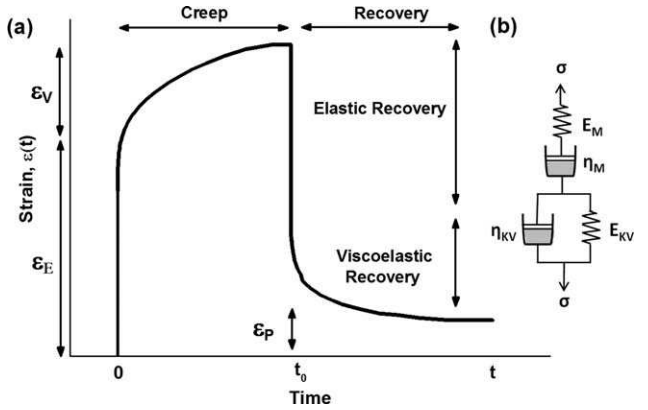

FIG. 7. (a) Typical creep-time diagram with three distinct strains and (b) Four-element (Burger's) sprig-dashpot viscoelastic model.

preceding results indicate that an increase in the CNC content in the nanocomposite reduced both the instantaneous elastic deformation and the time-dependent creep characteristic of the samples due to higher modulus of the samples. In other words, the presence of CNC particles imposed a physical constraint on the matrix chains that prevented the molecular motion and chain slippage which is responsible for the irrecoverable creep deformation. This chain motion restriction just mentioned is caused by the high stiffness of the CNC particles and strong interfacial interactions through hydrogen bonding. This observation and explanation are consistent with the reported work of Seltzer et al. [8] that showed that organoclay aluminosilicate particles reduced the time-dependent creep compliance and enhanced elasticity and rigidity of a polyamide 6 matrix. The fact that these rigid cellulose nanocrystals can beneficially reduce the time-dependent creep compliance, which is associated with the retardation of polymer chains under static load, encouraged us to further study these systems through appropriate theoretical models to quantify the viscoelastic parameters of these samples.

Theoretical Modelling of the Creep Process

A number of theoretical models in the literature have been used to interpret the polymer creep process and to predict the long-term creep behavior under experimental conditions that are inaccessible in the laboratory. One of the successful models used for this purpose is the so-called four element model known as the Burger's model [46, 47]. As depicted in Fig. 7, this viscoelastic model [48] (i.e., Burger's model) is composed of a Maxwell and Kelvin-Voight elements connected in a series arrangement. The total strain in the Burger's model is a sum of three separate parts; an elastic deformation (ε_E), a viscoelastic time-dependent strain (ε_V) and an irrecoverable permanent deformation due to viscoplastic flow of the polymer chains (ε_P). This total strain is formulated [46] as follows (Fig. 7a,b):

$$\varepsilon_{\text{Total}}(t) = \varepsilon_E + \varepsilon_V(t) + \varepsilon_P(t) \tag{1}$$

$$\varepsilon(t) = \frac{\sigma_0}{E_M} + \frac{\sigma_0}{E_M}\left(1 - \exp\left(\frac{-t.E_K}{\eta_K}\right)\right) + \frac{\sigma_0}{\eta_M}\cdot t \tag{2}$$

In this *Eq. 2*, the t is the time, E_M and η_M are respectively the spring modulus and dashpot viscosity of the Maxwell element, the E_K and η_K are the respective spring modulus and viscosity of the dashpot in KV element. The retardation time (i.e., $\tau_d = \eta_K/E_K$) corresponds to the time required to reach 63.2% of the total equilibrium deformation in the KV unit.

In this study, the obtained experimental data from the creep experiment at 25°C were fitted to the Burger's model using the nonlinear regression analysis curve fitting function of OriginPro 9.1® software and the calculated fitting parameters are shown in Table 2 with a correlation coefficient (R^2 value) greater than 0.99. The fitting curve is shown in Fig. 8a which shows a good agreement between the model and the experimental data. Table 2 shows that the values of all parameters show an increasing trend with increasing CNC content in the matrix. The E_K parameter corresponds to the instantaneous elastic deformation and is associated with elastic modulus of the Maxwell spring that increased from 2.1 GPa to 3.4 GPa by addition of 2 wt% of CNC particles. The elasticity of the KV element (E_{KV}) shows improvement by addition of the CNCs. This parameter has been reported to be associated with the amorphous fraction of a semicrystalline polymer matrix [46]. Now by considering the values of η_K and the retardation time (τ_d) it can be seen that both parameters increased by addition of the CNC. The obtained increase in the retardation time suggests that the viscoelastic relaxation of chains is significantly delayed upon incorporation of CNC particles. The viscosity of the dashpot in the Maxwell element (η_M) has been shown [48] to be associated with the permanent deformation due to the irrecoverable deformation. The higher value of η_M indicates a higher resistance of the composite against the viscoplastic flow (permanent deformation) with increasing the CNC content. Similar observations have been reported for polyurethane (PU)/CNC [46] shape memory systems where addition of small fractions of CNC to PU matrix

TABLE 2. Parameters of Burger's model fit (creep process) and Weibull distribution function fit (recovery process).

Model/CNC content (wt%)		0	0.6	1	2
Burger's model (Creep)	E_M (GPa)	2.09	2.23	2.81	3.45
	E_{KV} (GPa)	8.21	9.34	11.89	14.65
	η_{KV} (MPa s)*10^{-5}	9.9	12.9	24.2	43.8
	η_M (MPa s)*10^{-7}	2.1	2.5	4.2	6.8
	τ_d (s)	121	137.8	203.1	302.6
Weibull Distribution function (Recovery)	ε_V (%)	0.12	0.096	0.058	0.037
	η_r	339.4	390.6	702.7	645.5
	β_r	0.37	0.37	0.41	0.53
	Perm. Def. by model (%)	0.047	0.047	0.024	0.007
	Experimental perm. Def. (%)	0.061	0.057	0.032	0.011

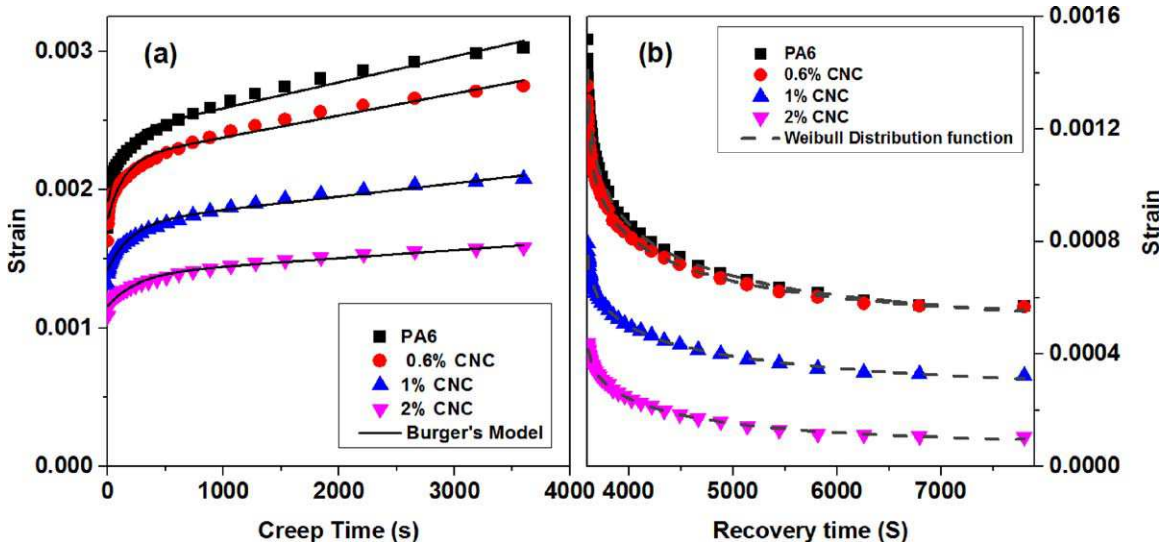

FIG. 8. (a) Burger's model fit on experimental data (b) Weibull distribution function fit on recovery process data. [Color figure can be viewed in the online issue, which is available at wileyonlinelibrary.com.]

reduced both the plastic deformation and overall creep strain. Other stiff and rigid nano-additives such as carbon nanotubes have also been reported in the literature to effectively reduce the plastic deformation of thermoplastic [46] and thermoset polymers [48].

The recovery process after the creep deformation is typically characterized by three stages. First an instantaneous recovery due to the elastic portion followed by a viscoelastic time dependent recovery, and a final permanent strain or irrecoverable deformation. In order to interpret and quantify this process, the Weibull distribution function [49] was used here to fit the experimental data based on the following equation (see Fig. 9):

$$\varepsilon(t)=\varepsilon_V\left[\exp\left(-\left(\frac{t-t_0}{\eta_r}\right)\right)\right]+\varepsilon_p \tag{3}$$

In this equation, the ε_V is the time dependent viscoelastic recovery strain, the η_r is the characteristic life, the β_r is the shape factor, t is time, t_0 is the time when the stress is removed and the ε_P is the permanent deformation. Clearly, the viscoelastic strain and the permanent deformation is reduced by addition of CNCs which signifies the fact that the recovery process is enhanced and the nanocomposites show higher tendency towards recovery after deformation. A good fitting of the model to the experimental data ($R^2>0.99$) was obtained (Fig. 8b) and the obtained fit parameters are shown in Table 2. As can be seen in this Table, the increase in shape factor and characteristic life shows that the nanocomposite tends to reach the equilibrium final strain value more quickly (i.e., shorter time-dependent recovery stage). This enhancement in the ability of the nanocomposites to recover the deformation after the load removal is associated with improved dimensional stability in load bearing applications which is a result of the incorporation of a small amount of CNC in the PA6 matrix.

Note that by comparing the final permanent deformation in experimental results to that predicted by the Weibull distribution model, a very good agreement can be seen and also we can see that 60 minutes of recovery time is not sufficient for the samples to reach the final equilibrium permanent deformation which is suggested by the model. It is interesting to see that the final values of experimental results are closer to the values predicted by the model for samples with higher CNC content. This shows that the CNCs contribute towards the faster and more efficient recovery of the strain in polyamide 6-based nanocomposite samples. In other words, the equilibrium final permanent deformation is reached faster as the CNC content is increased in the matrix.

Time-Temperature-Superpositioning of Creep Data. Time-temperature superposition (TTS) principle [50] has been successfully and widely used to predict the viscoelastic behavior of polymeric materials at long times or elevated temperatures that are experimentally inaccessible [46, 51, 52]. In the current research, the creep experiments were performed on all samples at five different temperatures namely 25°, 50°, 75°, 90°, and 105°C which covers a temperature range (T) below and above the glass transition ($T_g \sim 65$°C) (i.e., $T = T_g \pm 40$°C).

In the case of semi-crystalline polymers or filled polymer systems, typically the conventional equations (such as WLF equation) do not provide accurate predictions due to the thermorheological complexity of the materials near T_g [53–55]. In order to optimize the superposition process, usually a vertical shift factor is applied in conjunction with a horizontal shift factor to compensate for the drastic change in the initial instantaneous change of the studied viscoelastic property caused by the temperature change.

Since α_T cannot be predicted accurately based on the above explanation, the shifting can be carried out in an objective manner like the one reported by Honerkamp and Weese [56]. In this study, the TTS option of Thermal Advantage software provided by TA Instruments® was used for shifting purposes. The

 DOI 10.1002/pen

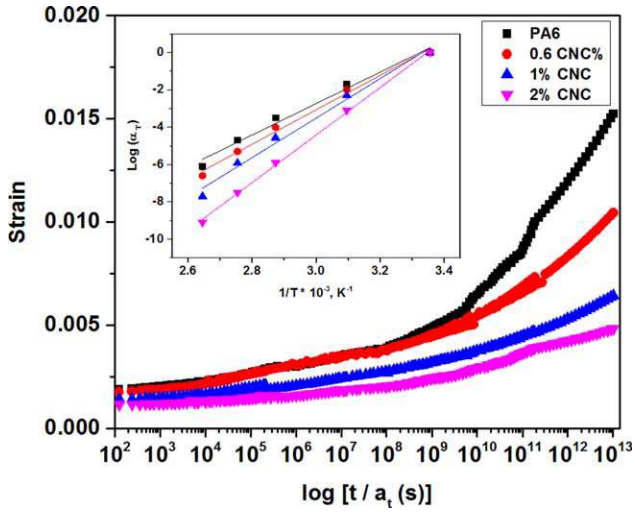

FIG. 9. Master curves showing the creep strain as a function of time and the horizontal shift factors with the linear fit according to the Arrhenius equation. [Color figure can be viewed in the online issue, which is available at wileyonlinelibrary.com.]

horizontal shift factor can be studied in the form of an Arrhenius equation as follows:

$$\log(a_T) = \frac{\Delta E}{2.303R}\left(\frac{1}{T} - \frac{1}{T_0}\right) \quad (4)$$

where the ΔE is the activation energy, R is the gas constant, T is the temperature, and T_0 is the references temperature (chosen here to be 25°C).

The obtained shifted curves are shown in Fig. 9. As can be seen in this figure, an acceptable superposition is obtained. The creep strain of PA6 matrix and nanocomposites are predicted to an extended time of 10^{13} s. By increasing the CNC content in the matrix, it is seen that at extended times the creep resistance is improved and the total strain is reduced. It is interesting to note that at a high level of expected time scale (more than 10^9 s) the significance in the creep strain difference between the matrix and nanocomposite of 0.6 wt% becomes more detectable which is basically due to the fact that the matrix enters the viscoelastic state and the reinforcing effect of cellulose nanocrystals even at very low content plays a significant role in improving the creep resistance.

The effect of molecular relaxation and chain slippage in presence of CNCs can be studied through the comparison of activation energies obtained from the linear regression of Arrhenius equation in Fig. 9 that shows the variation of shift factor with respect to temperature. The activation energies increased from 161.3 kJ/mol in the neat PA6 matrix to 243.9 kJ/mol in the 2 wt% CNC composite. For the nanocomposite samples of 0.6 and 1 wt% of CNC, the activation energies are respectively 176.5 and 202.7 kJ/mol. It is interesting to note that in a number of reported studies in the literature such as that of Yao et al. [48] on polyurethane/CNT systems and of Wu and co-workers on poly (butylene terephthalate/montmorillonite) nanocomposites [57], the authors found that the addition of nano-fillers into the polymer matrix did not result in significant changes in activation energies They attributed this observation to the fact that the poor interfacial interaction between the filler and matrix does not contribute to the creep resistance improvement but rather, the particles themselves form a network that resist the deformation. However, the results of the current study shows that the CNC particles are, in fact, inhibiting the chain relaxation and molecular motion through strong interfacial adhesion arising from hydrogen bond formation between the hydroxyl rich surface of cellulose nanocrystals and amide groups on the polyamide 6 backbone structure that is facilitated by the ROP processing method used. Therefore, it can be argued that both the presence of relatively tiny amounts of stiff and rigid CNC particles, as well as, the molecular motion retardation effect through interfacial interaction, improves the creep resistance of PA6/CNC nanocomposite materials.

Melt Rheological Studies

Because the melt rheological experiments were performed at 226°C, it was necessary to investigate plausible thermal degradation of the CNC particles in the samples during the measurements. For this purpose, a dynamic time sweep test was carried out to analyze the changes in storage and loss modulus of the neat polyamide 6 and the sample with 2% CNCs over time. PA6 is very well known to be thermally unstable in molten state. As shown in Fig. 10, there is an about 15% reduction in the G' parameter of the neat PA6 sample over a period of 10 min. For the nanocomposite sample with 2% CNC however, the storage modulus was found to decrease by average of 6% after 10 min indicating a synergistic improvement in thermal stability of the viscoelastic properties upon addition of the CNC in the PA6 matrix. In order to prevent the interference of the thermal instability with rheological experiments, all the melt rheological experiments were limited to around a total time duration of 10 min so that effects of thermal degradation can be minimized.

Small amplitude oscillatory shear experiments were carried out in order to probe the effect of the CNCs on the melt flow properties of the PA6 matrix and the obtained results are shown in Fig. 11a–c. As can be seen in this figure, increasing the CNC content increased the elastic modulus of the PA6 matrix, being more pronounced in the low frequency region. Note that it is

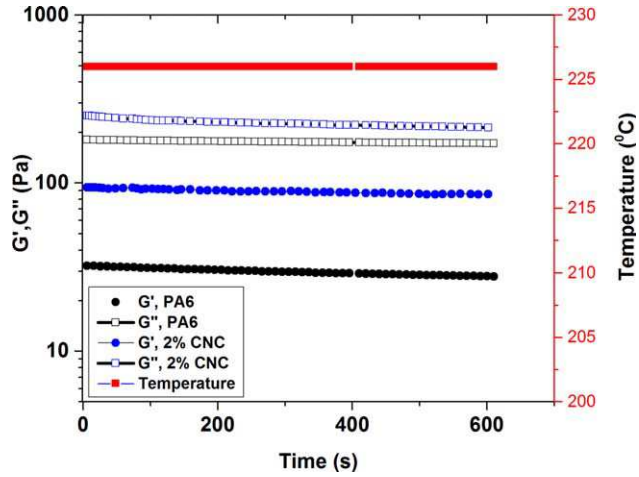

FIG. 10. Dynamic time sweep test for evaluation of the thermal stability of the viscoelastic properties in neat PA6 and 2%CNC nanocomposite samples at 226°C. [Color figure can be viewed in the online issue, which is available at wileyonlinelibrary.com.]

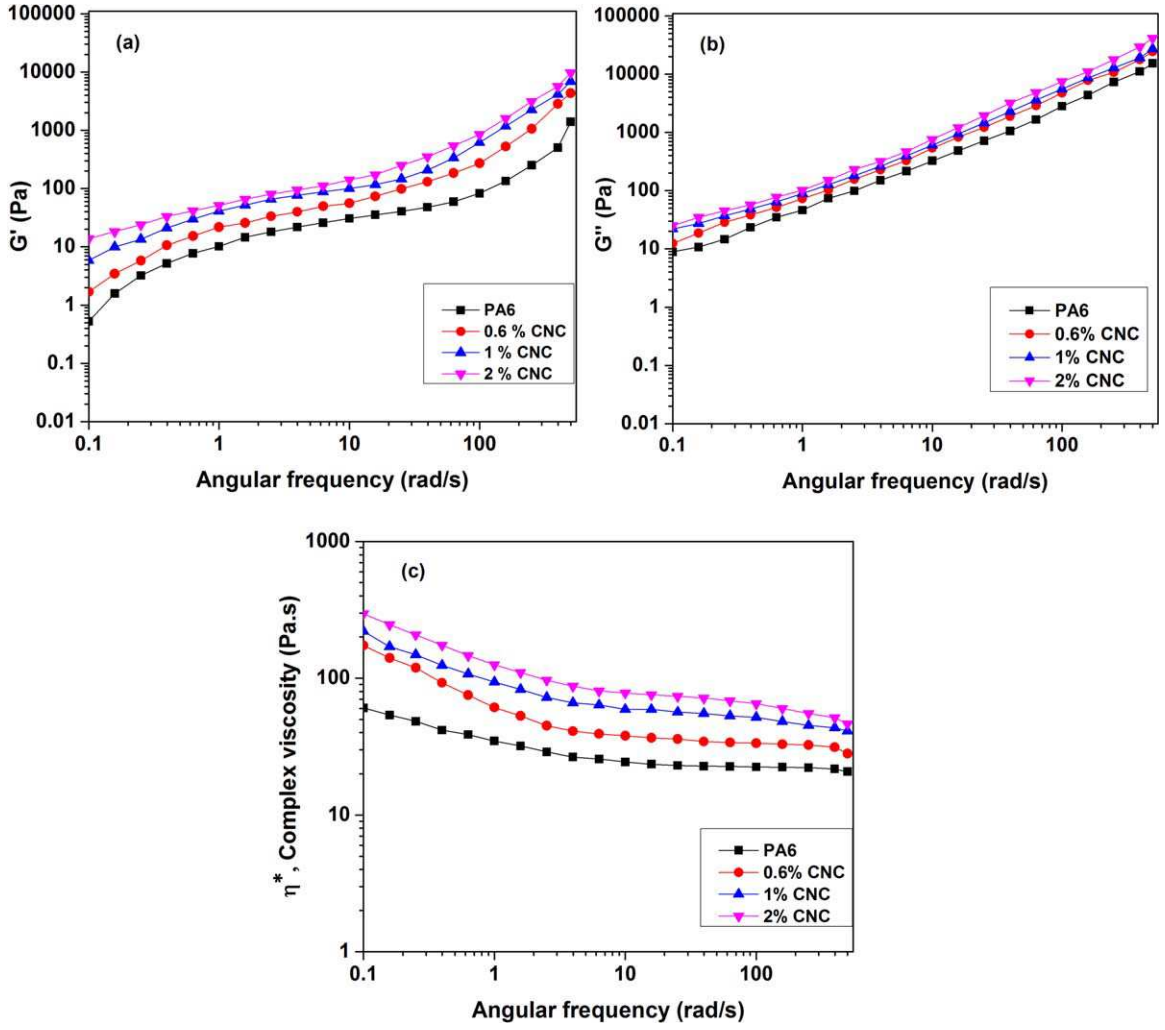

FIG. 11. Variation of (a) storage modulus, (b) loss modulus and (c) complex viscosity versus angular frequency for PA6 and PA6/CNC nanocomposites. [Color figure can be viewed in the online issue, which is available at wileyonlinelibrary.com.]

well known that in filled polymer systems, a nonterminal rheological behavior of the sample at low frequency is indicative of formation of a particle-induced structure to an extent that depends of the polymer/particle interactions [58]. Clearly, in the whole frequency range examined, the sample with 2% CNC showed higher elastic modulus, indicating significant elastic contribution of the CNCs in the melt. The nonterminal nature of the rheological behavior can be studied through the slope of the G' vs. ω at the low frequency region which can in turn be effectively used to interpret the structure development [59]. For this purpose, a linear regression of an exponential function of modulus and frequency ($G \propto \omega^n$: $\ln(G) = n \ln(\omega)$ was performed in the frequency region of 0.1–1 rad/s and the obtained results are shown in Table 3. This table shows that the terminal slope changed from 1.46 in the pure PA6 matrix to 0.72 in the sample with 2% CNC. A similar trend was observed for the G'' curve where the terminal region slope changed from 0.87 in the pure matrix to 0.54 in the sample with 2% CNC. This observed decreasing trend in slope with increasing CNC content can be explained by microstructural changes in the samples. With increasing content of CNCs and consequent strong polymer-particles and inter-particles interactions, a structural network is developed that shows a pseudo-solid-like behavior, especially in low frequency regions, due to the significant restriction imposed on polymer chains [60, 61]. Similar to the discussion on the solid-state tan δ variations at low frequency region already discussed, the polymer chains can relax under the dynamic load due to a relatively large response time. However, the influence of elastic contributions in the melt resulting from the 3D network of stiff CNCs, is evident in the low frequency regime of the dynamic frequency test results shown in Fig. 11.

It is interesting to note that in the high frequency region, the values of elastic modulus of the nanocomposite melts are slightly higher than that of the neat PA6. However, the nanocomposite samples showed quite similar values of elastic modulus. The experimental results just mentioned can be ascribed to the fact that the high frequency region is predominantly governed by short-range dynamics of polymer chains and the rheological behavior of the system is dominated by the matrix properties [62]. In contrast, in the low frequency region, the behavior of the materials is governed by relatively long-range interactions and the formation of CNC network, instead of the

 DOI 10.1002/pen

TABLE 3. Terminal region slope of elastic and loss moduli, Zero shear viscosities and terminal region slope of structure recovery test.

CNC content (wt%)	Slope of terminal G'	Slope of terminal G''	Zero shear viscosity (Pa s)	$T\infty$ *10^2
0	1.46	0.87	118.9	0
0.6	1.26	0.73	176.7	0.02
1	0.95	0.67	226.7	0.9
2	0.72	0.54	283.2	3.8

relaxation of matrix polymer molecules as the CNC network resists the structural relaxation which is responsible for the observed enhanced melt elasticity as already discussed. The variation in complex viscosity of samples versus frequency is shown in Fig. 11c. As expected, it can be seen from this figure that the nanocomposite samples showed higher complex viscosities compared to that of the neat PA6 especially at low frequencies.

At low frequency regions, the viscous flow dominates as the polymer chains are in their relaxed state, resulting in a terminal flow characteristic. This regime is governed by the power-law relationships of $G' \sim \omega^2$ and $G'' \sim \omega$ for homo polymers. However, as the CNC is added to the melt and the content is increased, a non-terminality of the flow at these low frequency regions develops and the storage and loss moduli become less dependent on the frequency. As already mentioned, this experimental fact just mentioned is primarily due to the development of an interconnected network of the CNC whiskers and associated pseudo-solid like flow behavior. This behavior is consistent with the lower slopes of G' and G'' and higher slope of complex viscosity at lower frequencies.

A similar type of behavior has been reported in the literature for polypropylene/CNC nanocomposites and PA6/carbon nanotube composites [58, 59]. Interestingly, in a comparative study reported by Tung and coworkers [35], PA6/nanoclay samples prepared by melt blending and *in situ* polymerization were compared for their melt rheological properties.

To better understand the structure of the nanocomposite samples of the current study and its interrelation with rheological properties, a number of steady shear experiments and coupled steady and dynamic experiments were performed. The obtained variation of viscosity versus steady shear rate is shown in Fig. 12. As can be seen in this figure, the nanocomposite samples showed higher absolute values of viscosity compared to that of neat PA6 matrix. Here, zero-shear viscosity values were approximated by the value at $0.001 s^{-1}$ and are tabulated in Table 3 for easy comparison. This table shows that this zero-shear viscosity value changed from 118.9 Pa s for the neat polymer to 283.2 Pa s for the nanocomposite with 2% of CNC particles.

At the relatively higher shear rates, the filled polymer systems showed onset of shear-thinning behavior at low shear rates compared to that of the neat polymer. Clearly, not only the onset of shear thinning behavior occurred at low shear rates for the filled polymer systems, but also the slope of the shear-thinning region is significantly higher for the nanocomposite samples, especially for the nanocomposite samples with 2% of CNC. In order to further elaborate on this point, the slope of the shear-thinning region was calculated for the neat polymer and the nanocomposite with 2% of CNC. The data points in the shear-thinning region were fitted using a power law function and the power law index was found using a linear regression of *Eq.* (5).

$$\tau = k\dot{\gamma}^{n} \rightarrow \eta = k\dot{\gamma}^{n-1} : \ln(\eta) = A + (n-1)\ln\dot{\gamma} \tag{5}$$

For the neat polymer the power law index (n) was found to be 0.37 while this value for the 2% CNC nanocomposite sample was 0.64. Therefore, the more shear-thinning characteristic of the CNC filled PA6 composites can be quantified using this power law index.

The empirical Cox-Merz rule has been shown to be an effective tool in studying the structure and flow properties of filled and unfilled polymer systems and have been widely used to correlate oscillatory dynamic experiments with steady shear experiments [63–65] and it has also been used in Polyamide 6 systems [66]. According to this rule, the absolute values of the viscosities in an oscillatory dynamic experiment should superimpose the value of steady shear experiment at identical frequencies and shear rates particularly at infinitely low angular frequencies (or shear rates) as shown below.

$$|\eta^*(\omega)_{\omega\rightarrow 0}| \approx |\eta(\dot{\gamma})_{\dot{\gamma}\rightarrow 0}| \tag{6}$$

Here, the viscosity values at $0.1\ s^{-1}$ (0.1 rad/s) were considered for neat PA6 and PA6/2% CNC samples. For the neat polymer, the viscosity values are 61.6 and 79 in oscillatory and steady shear experiments, respectively, indicating a slight difference (but reasonable correlation) between these values. This slight difference is due to the fact that there are strong intermolecular interactions in polyamide 6 (through hydrogen bonding). However, for the sample containing 2% CNC particles, the obtained viscosity value of 239.9 Pa s in oscillatory shear is significantly different from the value of 151.2 Pa s obtained in the steady shear experiment, indicating the failure of Cox-Merz rule. The Cox-Merz rule does not hold when there are specific elastic contributions in the melt. It is proposed here that the elastic contribution of CNC particles network is responsible for the failure of the Cox-Merz approximation. In the current study, it can be concluded that the presence of rigid CNC network and strong interaction of polyamide chains with the surface of the CNC

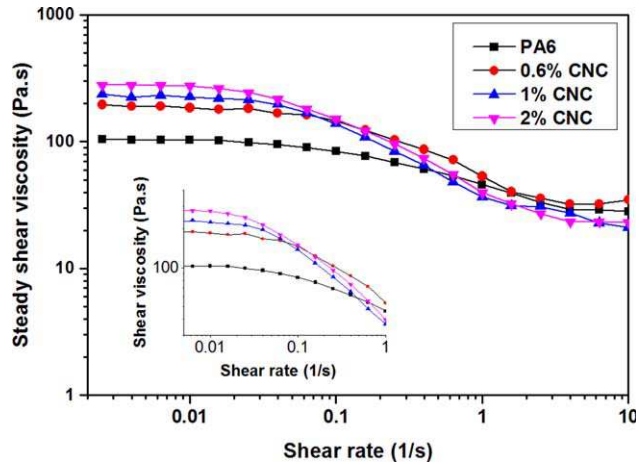

FIG. 12. Variation of shear viscosity versus shear rate for PA6 and PA6/CNC nanocomposites. [Color figure can be viewed in the online issue, which is available at wileyonlinelibrary.com.]

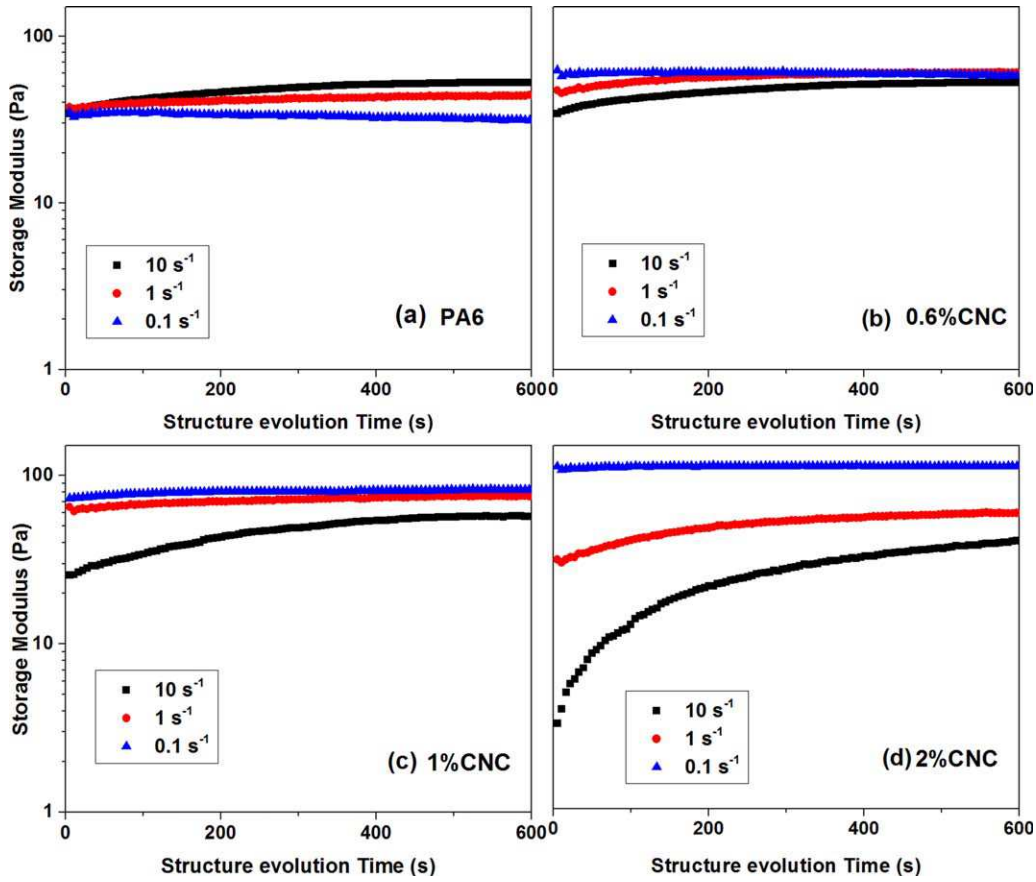

FIG. 13. Evolution of storage modulus over time after the pre-shearing stage for (a) PA6, (b) 0.6%CNC, (c) 1%CNC and (d) 2%CNC nanocomposites. (the values of pre-shear rate is shown in the insertion box for each graph). [Color figure can be viewed in the online issue, which is available at wileyonlinelibrary.com.]

particles results in significant elastic contribution to the melt properties (from the particles) which in turn results in deviation of the rheological behavior from that of neat matrix.

In order to investigate the structure formation of CNC particles in the polyamide 6 matrix, a series of real-time stress development experiments of pre-sheared samples were carried out in order to further look into the break-up and reformation of CNC network in the matrix. In Fig. 13 the development of elastic modulus (G') over time after a pre-shearing stage of 30 s (at three different shear rates) is shown. As can be seen, for the neat polymer sample, there is a minimal elastic recovery observed at all different pre-shear rates as the pre-shearing stage solely disrupts the chain entanglements and orient the chains in the flow direction; this again confirms that the pure PA6 sample shows a dominating viscous behavior with minimum elastic character. However for the filled systems a completely different behavior is observed.

In addition, all samples showed no changes in structure upon the application of 0.1 s^{-1} pre-shear because the melt elastic modulus of the samples remained almost constant throughout the 600 s experiment time. However, as the pre-shear rate was increased to 1 and 10 s^{-1} the initial modulus of the filled polymer samples dropped to lower values (as the shear rate increased). This shows that the application of shear results in break-up of the existing rigid structure in the sample and also orients the entangled polymer chains at the interface of cellulose nanocrystals, and consequently the elasticity (a measure of stiffness) of the melt is decreased. When the time sweep test starts, these disrupted structures find a second opportunity (in absence of intense shearing force) to aggregate and form new structures. As the CNC content of the melt increases, there is a significant reduction in the initial elastic modulus, and the change in elastic modulus covers a wide range over the experimental timescale investigated. In brief, as the CNC concentration increases, the elastic modulus of the sample drops more significantly after the pre-shear stage (indicated by lower start-up modulus in the subsequent time sweep test). In addition, there is a greater tendency in the sample with higher CNC content to recover the "elasticity" due to the structure formation of CNC particles in the melt once the shear is stopped.

The graphs shown in Fig. 13 clearly indicate that as the CNC content increases, the stiffness or elastic properties of nanocomposite melts becomes more dependent on the shear history of the samples. The more cellulose particles in the melt, the more structural clusters tend to form, which as a consequence, results in more dependency on the shear, only if the applied shear rate is high enough to break up the network. It can also be concluded from this behavior that the particle-particle affinity of the CNCs in the PA6 melt is more favorable than particle-polymer interactions, as the evolution of the elastic properties is

 DOI 10.1002/pen

due to the formation of agglomerates and clusters of the CNC particles (which is absent in the neat PA6 sample). Another important aspect of Fig. 13 that can be considered is the terminal regions of the structure recovery curves. As the Figure shows, increasing the shear rate increased the slope of the terminal region of curves (i.e., at 10 s^{-1}). The same trend was observed when the content of CNC particles was increased in the melt. In contrast, by lowering the shear rate and decreasing the CNC content, the curves appeared to reach their plateau modulus more quickly after which there is no increase in elastic modulus. To quantify this property of the studied materials, the terminal region slope (i.e., in the range of 500 − 600 s) of the curves pre-sheared at 10 s^{-1} is shown in Table 3. This slope shows the rate of evolution of G' in the terminal zone of the experiment. It is shown that as the CNC content in the melt increases, the structure recovery from the disrupted state to the steady state conditions requires longer time intervals. This implies that relatively long experimental times are required to reach the final plateau, but due to thermal degradation effects, the current experiments were limited to 600 s as already mentioned.

CONCLUSIONS

This study demonstrates feasibility of preparing novel polyamide 6 (PA6)/cellulose nanocrystal (CNC) nanocomposites via *in situ* anionic ring-opening polymerization reaction with improved creep resistance and enhanced dynamic mechanical properties, indicating the effective reinforcing ability of the CNCs as novel "green" reinforcement additives for engineering thermoplastic polymers such as PA6. The obtained results showed that the storage modulus of the PA6 matrix, which is a measure of stiffness of the nanocomposites, can be improved with addition of a relatively small amount of CNC particles ($\leq$2 wt% CNC). The creep resistance of the nanocomposites was improved by addition of the CNCs over a wide temperature range relative to T_g, as evidenced by the reduction in final creep strain, lower permanent deformation, and lower creep compliance compared with that of the neat PA6 matrix. Therefore, these novel thermoplastic nanocomposite materials may find uses in load-bearing applications where superior dimensional stability under constant load, light weighting, and favorable melt rheology (or processability) is crucial performance requirements.

A number of extant theoretical models in the literature were used to quantify the creep process and to interpret the changes caused by incorporation of the CNC reinforcement. The results of the theoretical modeling confirmed our expectation of enhanced elasticity due to the presence of a tiny amount of CNC particles in the thermoplastic matrix, which as a consequence, lowered the time-dependent viscoplastic flow and promoted the elastic recovery after the load removal. Time-temperature superpositioning was successfully applied to the creep data to predict the long-term creep behavior and it was found that the incorporation of the relatively rigid and stiff cellulose nanocrystals increased the activation energy of the molecular motion.

The melt rheological tests revealed enhanced melt viscoelastic material functions (i.e., melt viscosity, storage (elastic), loss modulus and complex viscosity). Significant stiffening of the polymer melt was exhibited by the 2% PA6/CNC nanocomposite, suggesting the onset of formation of percolated network structures and associated high shear thinning characteristics. Structure recovery tests showed that, provided a sufficiently high shear rate is applied, this network of CNC bundles can be broken apart followed by re-formation of the structure once the shear is removed. The observed increase in elastic properties of the PA6 melt containing CNCs increased over time is consistent with significant particle-particle affinity and bundle formation as evidenced by SEM images.

The cost-effectiveness, lightweight, renewability and environmental sustainability of the nanocomposites of this study compared to that of traditional glass or carbon fiber-reinforced (micro)composites may spur a better understanding of the current nanocomposites for a number of engineering applications where traditional carbon or glass fiber-reinforced polymer (micro)composites are not useable.

ACKNOWLEDGMENTS

The authors would like to thank Mithun Bhattacharya for assistance with AFM and Jessica Douglas for assistance with SEM imaging. The technical assistance of Dr René Fulchiron in data acquisition and analysis as well as access to rheological instrumentation in the Polymer Materials Engineering laboratory (IMP CNRS 5223) at University of Lyon 1 in France is gratefully acknowledged. J.U.O. gratefully acknowledges the U.S. Department of State, the French Ministry of Higher Education and Research, and the Franco-American Commission for jointly funding his Fulbright-Tocqueville Distinguished Chair award in Engineering at the University of Lyon 1; and IMP CNRS 5223 colleagues for their hospitality during his temporary residence in Lyon.

ABBREVIATIONS

CNC	cellulose nano-crystals
PA6	polyamide 6
ROP	ring opening polymerization
TTS	time temperature superposition

REFERENCES

1. I. Page, *Polyamides as Engineering Thermoplastic Materials*, Shropshire, UK: iSmithers Rapra Publishing, (2000).
2. D.P.N. Vlasveld, H.E.N. Bersee, and S.J. Picken, *Polymer*, **46**, 12539 (2005).
3. J.L. Yang, Z. Zhang, A.K. Schlarb, and K. Friedrich, *Polymer*, **47**, 2791 (2006).
4. M.M. Hasan, Y. Zhou, H. Mahfuz, and S. Jeelani, *Mater. Sci. Eng. A*, **429**, 181 (2006).
5. K. Varlot, E. Reynaud, M. Kloppfer, G. Vigier, and J. Varlet, *J. Polym. Sci. Part B: Polym. Phys.*, **39**, 1360 (2001).
6. Z. Xu and C. Gao, *Macromolecules*, **43**, 6716 (2010).
7. T. Liu, I.Y. Phang, L. Shen, S.Y. Chow, and W.D. Zhang, *Macromolecules*, **37**, 7214 (2004).
8. R. Seltzer, Y.W. Mai, and P.M. Frontini, *Compos. B*, **43**, 83 (2012).
9. H. Wei, K. Rodriguez, S. Renneckar, and P. J. Vikesland, *Environ. Sci.: Nano*, **1**, 302 (2014).

10. J.H. Kim, B. Shim, H. Kim, Y.J. Lee, S.K. Min, D. Jang, Z. Abas, and J. Kim, *Int. J. Precis. Eng. Man.*, **2**, 197 (2015).
11. G. Gong, J. Pyo, A.P. Mathew, and K. Oksman, *Compos. Part A: Appl. Sci. Manuf.*, **42**, 1275 (2011).
12. S. Spoljaric, A. Genovese, and R.A. Shanks, *Compos. Part A: Appl. Sci. Manuf.*, **40**, 791 (2009).
13. R.J. Moon, A. Martini, J. Nairn, J. Simonsen, and J. Youngblood, *Chem. Soc. Rev.*, **40**, 3941 (2011).
14. L. Pranger and R. Tannenbaum, *Macromolecules*, **41**, 8682 (2008).
15. A. Pei, J.M. Malho, J. Ruokolainen, Q. Zhou, and L.A. Berglund, *Macromolecules*, **44**, 4422 (2011).
16. T. Wang and L.T. Drzal, *ACS Appl. Mater. Interfaces*, **4**, 5079 (2012).
17. R. Rusli, K. Shanmuganathan, S.J. Rowan, C. Weder, and S.J. Eichhorn, *Biomacromolecules*, **12**, 1363 (2011).
18. A. Kaboorani, B. Riedl, P. Blanchet, M. Fellin, O. Hosseinaei, and S. Wang, *Eur. Polym. J*, **48**, 1829 (2012).
19. M.L. Auad, V.S. Contos, S. Nutt, M.I. Aranguren, and N.E. Marcovich, *Polym. Int.*, **57**, 651 (2008).
20. K.A. Iyer, G.T. Schueneman, and J.M. Torkelson, *Polymer*, **56**, 464 (2015).
21. Y. Habibi, L.A. Lucia, and O.J. Rojas, *Chem. Rev.*, **110**, 3479 (2010).
22. A. Dufresne, *Molecules*, **15**, 4111 (2010).
23. K. Oksman, A. Mathew, and M. Sain, *Plast., Rubber Compos.*, **38**, 396 (2009).
24. A. Kiziltas, B. Nazari, D.J. Gardner, and D.W. Bousfield, *Polym. Eng. Sci.*, **54**, 739 (2014).
25. A. Kiziltas, D.J. Gardner, Y. Han, and H.S. Yang, *Thermochim. Acta*, **519**, 38 (2011).
26. A.C. Corrêa, E. de Morais Teixeira, V.B. Carmona, K.B.R. Teodoro, C. Ribeiro, L.H.C. Mattoso, and J.M. Marconcini, *Cellulose*, **21**, 311 (2014).
27. J.U. Otaigbe and W.G. Harland, *J. Appl. Polym. Sci.*, **36**, 165 (1988).
28. K. Van Rijswijk, J. Teuwen, H. Bersee, and A. Beukers, *Compos. Part A: Appl. Sci. Manuf.*, **40**, 1 (2009).
29. K. Van Rijswijk, A. Van Geenen, and H. Bersee, *Compos. Part A: Appl. Sci. Manuf.*, **40**, 1033 (2009).
30. K. Van Rijswijk, H. Bersee, A. Beukers, S. Picken, and A. Van Geenen, *Polym. Test.*, **25**, 392 (2006).
31. K. Van Rijswijk, H. Bersee, W. Jager, and S. Picken, *Compos. Part A: Appl. Sci. Manuf.*, **37**, 949 (2006).
32. A. Liu, T. Xie, and G. Yang, *Macromol. Chem. Phys.*, **207**, 701 (2006).
33. G. Rusu and E. Rusu, *Int. J. Polym. Anal. Charact.*, **15**, 509 (2010).
34. M. Yang, Y. Gao, H. Li, and A. Adronov, *Carbon*, **45**, 2327 2327 (2007).
35. J. Tung, R.K. Gupta, G.P. Simon, G.H. Edward, and S.N. Bhattacharya, *Polymer*, **46**, 10405 (2005).
36. J.R. Capadona, O. Van Den Berg, L.A. Capadona, M. Schroeter, S.J. Rowan, D.J. Tyler, and C. Weder, *Nat. Nano.*, **2**, 765 (2007).
37. G. Rusu and E. Rusu, *Int. J. Polym. Anal. Charact.*, **16**, 561 (2011).
38. G. Rusu and E. Rusu, *J. Optoelectron. Adv. Mater*, **11**, 673 (2009).
39. H. Liu and M.P.G. Laborie, *Cellulose*, **18**, 619 (2011).
40. W. Helbert, J. Cavaille, and A. Dufresne, *Polym. Compos.*, **17**, 604 (1996).
41. A. Woodward, J. Sauer, C. Deeley, and D. Kline, *J. Colloid Sci.*, **12**, 363 (1957).
42. K. Pramoda and T. Liu, *J. Polym. Sci. Part B: Polym. Phys.*, **42**, 1823 (2004).
43. S. Zulfiqar, M. Ishaq, and M.I. Sarwar, *Surf. Interface Anal.*, **40**, 1195 (2008).
44. C. Zhao, G. Hu, R. Justice, D.W. Schaefer, S. Zhang, M. Yang, and C.C. Han, *Polymer*, **46**, 5125 (2005).
45. L. Shen, Q. Du, H. Wang, W. Zhong, and Y. Yang, *Polym. Int.*, **53**, 1153 (2004).
46. Y. Jia, K. Peng, X. Gong, and Z. Zhang, *Int. J. Plast.*, **27**, 1239 (2011).
47. I. M. Ward and J. *Sweeney: Mechanical Properties of Solid Polymers*, Wiley, West Sussex, United Kingdom, (2012).
48. Z. Yao, D. Wu, C. Chen, and M. Zhang, *Compos. Part A: Appl. Sci. Manuf.*, **50**, 65 (2013).
49. K.S. Fancey, *J. Mater. Sci.*, **40**, 4827 (2005).
50. J.D. Ferry, *Viscoelastic Properties of Polymers*, 3rd ed. New York: Wiley, (1980).
51. H.Z. Ding and Z. Wang, *Cellulose*, **14**, 171 (2007).
52. E.A. Osman and S.A. Mutasher, *Int. J. Comput. Mater. Sci. Eng*, **3**, 1450004 (2014).
53. A. E. Likhtman, *Viscoelasticity and Molecular Rheology*, Elsevier BV: Amsterdam, (2012).
54. M. Tajvidi, R.H. Falk, and J.C. Hermanson, *J. Appl. Polym. Sci.*, **97**, 1995 (2005).
55. J. Dealy and D. Plazek, *Rheol. Bull.*, **78**, 16 (2009).
56. J. Honerkamp and J. Weese, *Rheol. Acta.*, **32**, 57 (1993).
57. D. Wu, C. Zhou, Z. Hong, D. Mao, and Z. Bian, *Eur. Polym. J*, **41**, 2199 (2005).
58. V. Khoshkava and M.R. Kamal, *ACS Appl. Mater. Interfaces*, **6**, 8146 (2014).
59. M. Wang, W. Wang, T. Liu, and W.D. Zhang, *Compos. Sci. Technol.*, **68**, 2498 (2008).
60. C.A. Mitchell, J.L. Bahr, S. Arepalli, J.M. Tour, and R. Krishnamoorti, *Macromolecules*, **35**, 8825 (2002).
61. Y.T. Sung, M.S. Han, K.H. Song, J.W. Jung, H.S. Lee, C.K. Kum, J. Joo, and W.N. Kim, *Polymer*, **47**, 4434 (2006).
62. T.D. Fornes, P.J. Yoon, H. Keskkula, and D.R. Paul, *Polymer*, **42**, 09929 (2001).
63. W. Cox and E. Merz, *J. Polym. Sci.*, **28**, 619 (1958).
64. J.M. Dealy and R.G. Larson, *Molecular Structure and Rheology of Molten Polymers*, Hanser, Munich, (2006).
65. D.W. Mead, *Rheol. Acta.*, **50**, 837 (2011).
66. A. Guštin, A. Zupančič, and E. Mitsoulis, *J. Appl. Polym. Sci.*, **100**, 1577 (2006).